A Multi-omics Strategy Enabled by Sequential Metabolomics and Proteomics for Human Pluripotent Stem Cell-derived Cardiomyocytes

Elizabeth F. Bayne[1], Aaron D. Simmons[2], David S. Roberts[1], Yanlong Zhu[3,4], Timothy J. Aballo[3,5], Benjamin Wancewicz[3], Sean P. Palecek[2*], Ying Ge[1,3,4*]

[1]Department of Chemistry, University of Wisconsin-Madison, Madison, WI 53706, USA

[2]Department of Chemical and Biological Engineering, University of Wisconsin-Madison, Madison, WI 53706, USA

[3]Department of Cell and Regenerative Biology, University of Wisconsin-Madison, Madison, WI 53705, USA

[4]Human Proteomics Program, School of Medicine and Public Health, University of Wisconsin-Madison, Madison, WI 53705, USA

[5]Molecular and Cellular Pharmacology Training Program, University of Wisconsin-Madison, Madison, WI 53705, USA

*To whom correspondence should be addressed: Dr. Ying Ge, 1111 Highland Ave., WIMR II 8551, Madison, WI 53705. Email: ying.ge@wisc.edu. Tel: 608-265-4744. Dr. Sean Palecek, 1415 Engineering Drive, Madison, WI 53706. Email: sppalecek@wisc.edu. Tel: 608-262-8931.

1

Abstract

Human pluripotent stem cell-derived cardiomyocytes (hPSC-CMs) have shown immense promise for patient-specific disease modeling, cardiotoxicity screening, and regenerative therapy development. However, hPSC-CMs in culture have not recapitulated the structure or functional properties of adult CMs *in vivo* thus far. To gain global insight into hPSC-CM biology, we introduce a multi-omics strategy for analyzing the hPSC-CM metabolome and proteome from the same cell culture, creating multi-dimensional profiles of hPSC-CMs. Here we developed a sequential extraction to capture metabolites and proteins from hPSC-CM monolayer cultures, and analyzed these extracts using high resolution mass spectrometry (MS). Using this strategy, we identified an average of 205 metabolites/lipids and 4,008 protein groups from 10^6 cells with high reproducibility. We further integrated the proteome and metabolome measurements to create network profiles of molecular phenotypes for hPSC-CMs. Out of the 310 total pathways identified using metabolomics and proteomics data, 40 pathways were considered significantly overrepresented (FDR-corrected $p \leq 0.05$). Highly populated pathways included those involved in protein synthesis (ribosome, spliceosome), ATP generation (oxidative phosphorylation), and cardiac muscle contraction. This multi-omics method achieves deep coverage of metabolites and proteins, creating a multidimensional view of the hPSC-CM phenotype. This strategy can be used to generate biological hypotheses and identify biomarker candidates to advance the understanding of hPSC-CM differentiation and maturation.

Introduction

Human pluripotent stem cell-derived cardiomyocytes (hPSC-CMs) have shown immense promise for patient-specific disease modeling, cardiotoxicity screening, and regenerative therapy development [1-5]. Enabled by recent advances, hPSC-CMs can now be generated consistently with high yield and purity at a clinically relevant scale [6-9]. However, one of the roadblocks impeding the realization of the full potential of hPSC-CMs is their structural and phenotypic immaturity compared to adult CMs [9, 10]. Significant efforts have been made to mature hPSC-CMs and considerable progress has been achieved; nevertheless, hPSC-CMs still lack adult-like phenotypes *in vitro* [9, 11]. As hPSC-CM maturation entails complex signaling networks, new discovery approaches are urgently needed to gain systems-level insights into hPSC-CM biology [9, 12, 13].

High-throughput "omics" technologies provide transformative insights to elucidate complex biological processes. Conceivably, a multi-omic strategy will offer a more comprehensive understanding of hPSC-CM complexity than any single omic technology alone [14-17]. In the post-genomic era, proteomics and metabolomics offer an unbiased suite of tools to link proteins and metabolites for integrated analysis of signal transduction, cellular metabolism, and phenotype on a systems biology level [17-19]. Analysis of lipids, metabolites, and proteins from the same sample can provide precise insights to the phenotype from which they arise, and elimination of parallel sample processing mitigates concerns around batch variability [15, 20]. By measuring metabolites and proteins from the same hPSC-CM monolayer sample, the amount of information is maximized from these costly and time-consuming cultures. However, a multi-omics method with the capability to analyze both metabolome and proteome from the same hPSC-CM culture remains lacking. There are still challenges associated with reproducible sample extraction for both

3

metabolomics and proteomics, as well as correlation of metabolite and protein measurements from the same cell culture.

Herein, we developed a novel multi-omics method enabled by a sequential extraction and high-resolution mass spectrometry (MS)-based metabolomics and proteomics to analyze monolayer cultures of hPSC-CMs. After acquisition of metabolite and protein measurements from the same cell culture, we create a multi-dimensional profile of molecular phenotypes of hPSC-CMs. This report represents the first integration of untargeted metabolomics and proteomics data from hPSC-CM monolayer cultures to identify prominent biological pathways of hPSC-CMs. We demonstrate high reproducibility in our metabolomics and proteomics measurements, which provides a strong technological foundation to better understand hPSC-CM biology.

Materials and Methods

hPSC and hPSC-CM Cell Culture and Validation: Human induced pluripotent stem cells (WTC11 cell line) were maintained and differentiated into cardiomyocytes using the GiWi protocol as described previously [21]. hPSC-CM differentiation efficiency was assessed in parallel wells by flow cytometry for cardiac troponin T (cTnT)-positive CMs on Day 16 of differentiation [21]. The resulting purity was $72 \pm 2\%$ cTnT+ (n=5) (**Figure S1**).

Sequential Extraction of hPSC-CM Culture: Metabolites and proteins were sequentially extracted using a solvent-based quench technique [22]. Cells were incubated in 1.0 mL cold (4ºC) 100% methanol for 1 minute to quench cellular metabolic activity. Subsequently, cells were scraped into a 1.5 mL microcentrifuge tubes in methanol, referred to as "Metabolite-Protein Mixture." Metabolite-Protein Mixture was vortexed for 10s and incubated for 10 min at 4 ºC. The Metabolite-

4

Protein Mixture was centrifuged for 5 min at 14,000 g, creating a metabolite-rich supernatant and protein-rich cell pellet. The pellet was rinsed with 200 µL DPBS. Metabolite and protein samples were dried under vacuum and stored at -80 ℃.

Untargeted Metabolomics of hPSC-CM: Metabolites were reconstituted in 1:1 methanol:water. FIE-FTICR MS-based metabolic fingerprinting was performed using a Waters ACQUITY UPLC M-Class System (Waters Corporation, Milford, MS, USA) coupled to a Bruker solariX 12T FTICR mass spectrometer (Bruker Daltonics, Bremen, Germany) without an LC column as described previously [23]. MS data were processed using MetaboScape v2021 and feature assignments were manually validated using DataAnalysis v4.3 (both Bruker Daltonics, Bremen, Germany). Bucket lists for data collected in positive and negative ionization modes were generated using the T-Rex 2D algorithm and combined to create one merged bucket list using a mass error tolerance of < 1.0 ppm. Features were annotated by SmartFormula in MetaboScape as described previously [24] and by accurate mass using the Mass Bank of North America, Human Metabolome Database (HMDB) [25], LipidBlast [26], and METLIN databases [27] with an error tolerance ≤ 3.0 ppm. Overlap in metabolite features between hPSC-CMs was visualized using BioVenn [28]. Metabolites were mapped to networks using MetScape plugin in CytoScape v 3.8.1 [29].

Global Proteomics Analysis of hPSC-CM: Proteins from the dried cell pellet were solubilized in 10 µL buffer containing 0.25% w/v Azo. Samples were normalized, reduced, alkylated, and digested with Trypsin Gold (Promega, Madison, Wisconsin, USA). Samples were quenched and irradiated at 305 nm for 5 min, desalted and dried under vacuum.

Nanoflow LC-MS analysis of tryptic peptides was performed using a timsTOF Pro [30] coupled to a nanoElute nano-flow UHPLC system using a Captivespray nano-electrospray ion source all Bruker Daltonics, Bremen, Germany). The timsTOF Pro was operated in Parallel

5

Accumulation and Serial Fragmentation (PASEF) mode. Tandem mass spectra were searched against the UniProt human database UP000005640 using MaxQuant v1.6.17.0 [31] using a false discovery rate of 0.01. Label free quantification (LFQ) was performed using classic normalization and a minimum ratio count of 2. To determine correlation of LFQ intensities across samples, Perseus software v1.6.14.0 [32] was used to transform the data by log2x and generate scatter plots with Pearson correlation coefficients. Overlap in protein groups and peptides identified between hPSC-CMs was visualized using BioVenn. Pathway analysis of proteins identified in the dataset was performed using the ReactomeFI plugin for Cytoscape [33].

Multi-omics (Metabolomics-Proteomics) Data Integration: Protein (UniProt identifications) and metabolite (KEGG identifiers) lists were uploaded to MetaboAnalyst 5.0 for integrative pathway analysis [34]. The Joint Pathway Analysis module was used to determine significantly enriched pathways within the dataset (hypergeometric test, $p \leq 0.05$).

For further details, refer to **Supplemental Materials and Methods.**

Results and Discussion

A Multi-Omics Platform

We have developed a novel multi-omics platform to analyze metabolites (including lipids) and proteins from the same hPSC-CM sample. To harvest metabolites and proteins, cellular activity was quenched using cold methanol [22], simultaneously extracting metabolites and precipitating proteins (**Figure S2**). This quenching protocol achieves rapid, reproducible access to the metabolome and proteome. After a brief centrifugation step, the metabolite-rich supernatant and the dehydrated cell pellet were easily separated and analyzed using MS-based metabolomics and proteomics, respectively. The supernatant required no further preparation prior to analysis by

6

MS-based metabolomics, while the cell pellet was resolubilized using Azo before the analysis by the MS-based proteomics. Direct metabolite extraction using methanol was chosen over traditional cell-lifting based protocols as it has been shown to better preserve endogenous intracellular metabolite profiles [35].

We used several specialized analytical approaches to enable a high throughput and comprehensive analysis of hPSC-CM metabolites and proteins. To measure metabolites, we used an automated flow injection electrospray (FIE) platform integrated to Fourier transform ion cyclotron resonance (FTICR) MS [24]. The ultrahigh mass accuracy and resolving power of the FTICR MS enable simultaneous detection and quantification of complex mixture of metabolites without the need for chromatographic separation, sample fractionation, or chemical derivatization, resulting in metabolite identifications with sub-ppm mass accuracy and a high-throughput analytical workflow [24].

To solubilize proteins for global bottom-up proteomics, we used Azo [36], a novel photo-cleavable surfactant that enables high-throughput enzymatic digestion. Further, minimal sample cleanup is required as <5 minutes of exposure to UV light will degrade it into MS-compatible products [23, 37]. Moreover, Azo has been shown to effectively access critical membrane and ECM proteins [23]. To analyze peptides, we used online data-dependent Parallel Accumulation-Serial Fragmentation (dda-PASEF) on the timsTOF Pro [38, 39]. The coupling of trapped ion mobility spectrometry (tims) with PASEF on the timsTOF Pro enables rapid sequencing of peptides, resulting in deep and sensitive proteome coverage using a standard 120 minute sample run [39].

High Resolution Untargeted Metabolomics enabled by FIE-FTICR MS Platform

Metabolite samples were directly infused into a 12 T FTICR MS using an automated flow injection and electrospray ionization (FIE-FTICR MS) (**Figure 1A, S2**). Our FIE-FTICR MS platform requires only 5 min of analysis time per sample and detects hundreds of metabolite features with high mass accuracy (**Figure S3A**). Additionally, the FIE-FTICR MS platform can profile small molecule metabolites as well as lipid composition of the sample within this 5 min analysis. FIE-FTICR MS enables fast polarity switching, allowing for more access to unique metabolites in the sample, including amino acids, alkenes, and ceramides in the positive mode and a variety of phospholipid classes in the negative ionization mode (**Figure S3B**). From approximately 10^6 cells, we detected an average of 626 metabolite features between positive and negative ionization modes. Of those features, 468 were annotated by the SmartFormula (SF) function in MetaboScape with ≤ 5.0 ppm mass error tolerance, generating a putative chemical formula based exact mass and isotopic pattern. In a representative zoomed-in window of the mass spectrum ranging from 180-250 *m/z* showed 14 SF annotations made within 5 ppm error in positive ionization mode, with 12 features annotated with errors around 2 ppm (**Figure S4A**). In the negative ionization mode, 12 features were annotated by SF in the same 70 *m/z* window within 5 ppm error, with 7 of them annotated with an *m/z* error tolerance of < 1 ppm (**Figure S4B**). Metabolites were annotated from databases such as METLIN and Mass Bank of North America were annotated using high mass accuracy (≤ 3.0 ppm). These annotations cover a broad range of metabolites and lipids, including triglycerides (TAG), ATP, NADH, and UDP-glucose (**Figure 1B**).

We demonstrated highly reproducible injections for the analysis of hPSC-CM metabolites (**Figure S5A**). Mass spectra of triplicate injections show similarity in metabolite feature intensity

8

and populations in both positive and negative ionization modes. After a blank reduction step, 624-629 features were detected in each injection replicate and shared 623 features in common, corresponding to over 99% overlap between triplicate injections (**Figure S5B**). Variation in shared feature intensities was low, with 6.9% median relative standard deviation (RSD) for all features detected. 96% of features detected had a signal intensity variation less than 20% RSD and 72% of features less than 10% RSD (**Figure S5C**). We used this strong technical foundation to evaluate the reproducibility of hPSC-CM metabolite extraction using biological replicates (n=3). Visual comparison of mass spectra shows similar intensities and feature population between hPSC-CM biological replicates in both ionization modes (**Figure S6A**). 619-623 features were detected in 3 of 3 triplicate injections for each biological replicate and 613 features were shared between them, corresponding to 98% overlap of features detected between biological replicates (**Figure S6B**). Of these shared features, 459 were annotated with SF. Variation in feature intensity across biological replicates was 13% median RSD, and 84% of features varied by $\leq$ 20% RSD (**Figure S6C**). Taken with the high overlap in features detected between biological replicates and high technical reproducibility, these variation in the data indicate the methods' sensitivity to differences in metabolite profiles between hPSC-CMs.

Hundreds of metabolites important to hPSC-CM biology were identified in our dataset with high mass accuracy, involving pathways such as amino acid metabolism, glycolysis, and glycerophospholipid metabolism (**Figure 1C**). 205 metabolites were annotated using a combination of the METLIN, HMDB, LipidBlast, and MoNA databases with an error tolerance of $\leq$ 3.0 ppm. Of those metabolites, 46 were annotated with mass error tolerance of $\leq$ 0.2 ppm, and 117 were annotated $\leq$ 1.0 ppm. Energy-yielding substrates such as glucose, ATP, fatty acids, acyl-carnitines, amino acids, and triglyceride (TAG) species were detected in the dataset (**Table S1**),

9

which can be correlated to energy-generating pathways. Metabolites involved in oxidative phosphorylation (e.g. NAD+/NADH, ATP/ADP), a primary source for ATP generation in mature CMs [40, 41], were also consistently identified in the dataset (**Figure 1D**). Diverse phospholipid species including sphingolipids, ceramides, phosphocholines (PC), cardiolipins (CL), phosphotidylserines (PS), phosphotidylglycerols (PG), and phosphotidylethanolamines (PE) were also identified in the dataset. Phospholipids have been shown to play a key role in the position and function of membrane-embedded ion transporter proteins, which regulate cardiac contraction [42]. Thus, we can access a wide range of biologically relevant metabolite classes, from carbohydrates to lipids, using this fast and reproducible procedure to investigate active metabolic pathways in hPSC-CM biology.

Global proteomics of the hPSC-CM cell pellet

After metabolite extraction, we subsequently extracted proteins from the hPSC-CM cell pellet using label-free global bottom-up proteomics. The pellet was resolubilized in a buffer containing MS-compatible surfactant Azo [23], enzymatically digested, and analyzed by online LC-PASEF-MS using the timsTOF Pro (**Figure 2A, S2**) [39]. Technical reproducibility was demonstrated for the Azo-enabled bottom-up global proteomics method through similar protein yields for each pellet as demonstrated by Bradford assay, with protein yields of 26-31 μg of total protein per hPSC-CM sample (**Table S3**). Given that only 100-200 ng peptides are required for each bottom-up global proteomics run, this procedure yields adequate protein to analyze each hPSC-CM monolayer culture and could be scaled down to accommodate smaller monolayer cultures ($<10^6$ cells). The online data-dependent PASEF proteomics platform showed high technical reproducibility and robustness throughout the analysis. Over the course of 29 sample

10

injections (58 hours, 2.5 days), the maximum shift in retention time is only 0.2 min difference between injections of the K562 whole cell lysate standard at 200 ng at the beginning and end of the run, demonstrating impressive run-to-run reproducibility across multiple samples injections (**Figure S7A,B**). Additionally, label-free quantitation (LFQ) of the K562 cell standard showed strong correlation between three bracketing standard runs spanning 58 hours, with a Pearson correlation coefficient of 0.997 (**Figure S7C**).

Global proteomics revealed a large diversity in protein groups recovered from the cell pellet after the initial metabolite extraction. Analysis of online dda-PASEF bottom-up proteomics data using a false discovery rate (FDR) of 1% at the protein and peptide level revealed a total of 31,617 unique peptides between three hPSC-CM biological replicates, corresponding to 4,319 combined protein groups. Using only 200 ng per run, 21,240 peptides were shared between three hPSC-CM cultures (**Figure 2B**). We found 3,663 proteins in common between replicates, corresponding to 85% overlap between biological replicates (**Figure 2C**). Additionally, strong correlation of LFQ intensities show consistent recovery of proteins from the dual extraction, with Pearson correlation coefficients ranging from 0.960-0.983 (**Figure 2D**). Normal unimodal distribution of log transformed (LFQ) intensities was observed for each of the three replicates (**Figure 2E**). These results illustrate the reproducible extractions of proteins from the residual hPSC-CM pellet by this sequential extraction strategy and demonstrate the feasibility of applying this method for quantitation between samples from sequentially-extracted hPSC-CMs for metabolomics and proteomics.

Gene ontology analysis revealed highly diverse protein groups recovered from the sequentially-extracted hPSC-CM pellet. Protein groups within our dataset represented the majority of KEGG pathways using the Database for Annotation, Visualization, and Integrated Discovery

(DAVID) [43]. Using this tool, we found 91 KEGG pathways represented by the proteomics dataset. Among them, 65 pathways were considered abundantly represented (FDR-corrected $p \leq$ 0.05), many of which reflect ATP-generating pathways as well as cardiomyocyte function and development (**Table S5**). For example, two of the most significantly abundant pathways represented in the dataset, the Spliceosome and Ribosome, are relevant to protein processing and translation.

Proteins involved in metabolic pathways were highly represented throughout the dataset, constituting 417 total protein groups (**Figure 2F**). Among them, diverse pathways were identified, such as amino acid metabolism pathways and mitochondrial fatty acid β-oxidation. Glycolysis is responsible for the majority of ATP generation in the immature hPSC-CMs [40], and was represented by 37 proteins in the dataset, including hexokinase-1 (HK-1, gene: *HK1*), α-enolase (gene: *ENO1*), and pyruvate kinase (gene: *PKM*). Oxidative metabolism generates the majority of ATP in mature CM phenotypes [41], and mitochondrial pathways TCA cycle and oxidative phosphorylation comprised 24 and 74 proteins in the dataset, respectively, including each constituent of the membrane-embedded electron transport chain (**Figure 1D**). Fatty acid degradation comprised 24 proteins in the dataset, including mitochondrial proteins glutaryl-CoA dehydrogenase (gene: *GCDH*) and very long-chain specific acyl-CoA dehydrogenase (gene: *ACADVL*). Metabolism of amino acids and derivatives, including valine, leucine, and isoleucine degradation (hsa00280) and biosynthesis of amino acids (hsa01230) was represented by 39 and 48 proteins, respectively. The depth of coverage of metabolic protein groups and pathways in the hPSC-CM dataset can be used for metabolite annotations to analyze the cells from a multi-omics perspective.

Cardiac-specific proteins were also consistently detected throughout the dataset. Cardiac-specific pathways found in KEGG pathways included Cardiac Muscle Contraction (hsa02460) and Adrenergic Signaling in Cardiomyocytes (hsa02461) comprising 36 and 57 proteins, respectively (**Figure 2G**). Cardiomyocyte-specific marker cardiac troponin T (cTnT, gene: *TNNT2*) [8] was consistently detected in each CM replicate with 0.2% RSD in LFQ intensity (**Figure S11A**). Other cardiac proteins such as slow skeletal troponin I (ssTnI, gene: *TNNI1*), α-cardiac muscle actin (α-CAA, gene: *ACTC1*), cardiac troponin C (cTnC, gene: *TNNC1*), cardiac myosin binding protein C (gene: *MYBPC3*), cardiac phospholamban (gene: *PLN*), and cardiomyocyte transcription factor GATA-4 (gene: *GATA4*) [44] were consistently detected as well (**Figure S11 B-F**). Important cardiac contractile proteins and markers of CM specification were consistently identified, including the atrial and ventricular isoforms of myosin light chain (MLC-2a, gene: *MYL7* and MLC-2v, gene: *MYL2*, respectively), and α- and β-myosin heavy chains (α-MHC, gene: *MYH6*, β-MHC, gene: *MYH7*, respectively) (**Figure S11 G-J**). MLC-2v and MLC-2a are considered markers of development and the presence of MLC-2v can also indicate development of ventricular CM linages [10].

Importantly, a large number of proteins associated with the extracellular matrix (ECM) sub-proteome ("matrisome") were detected in the sequentially-extracted hPSC-CMs (**Figure 2G**). Cardiac ECM proteins are crucial to providing structural support to the CM monolayer and help to withstand mechanical stress from continual contraction of the sarcomere [45]. Key ECM proteins to CM function [45] were detected in the sequentially-extracted cultures, including collagen I (genes: *COL1A1*, *COL1A2*), collagen III (gene: *COL3A1*), and basement membrane proteins collagen IV (genes: *COL4A1, COL4A2, COL4A3* and *COL4A6*) and fibronectin (gene: *FN1*). Overall, core matrisome proteins [46] were consistently detected throughout the dataset,

including 21 collagen species, 62 glycoproteins, and 11 proteoglycans. We also detected 115 matrisome-associated proteins, which are ECM regulators and secreted factors, or are structurally affiliated with the ECM (Supplemental **File 1**) [46]. 43 proteins were associated with the KEGG pathway "ECM-receptor interaction" (hsa04512) including various subunits of the transmembrane integrin receptor complex (genes: *ITGB1* and *3*, *ITGAV*, and *ITGA1, 2,* and *5-7*), as well as α-, β-, and γ- chains of the laminin complex (genes: *LAMA1-LAMA5*, *LAMB1* and *2*, and *LAMC1* and *2*). The reliable detection of diverse matrisome species using a sequentially-extracted method is significant because protein solubility is the primary challenge of ECM proteomics [47, 48]. Often, multi-step extraction procedures are used to isolate the ECM. Using a single-step proteomics extraction enabled by Azo, we detected a diverse array of core and associated matrisome constituents in addition to the metabolic and sarcomeric subproteomes, enabling analysis of each subproteome on a global scale.

Integrative Multi-Omics Reveals Highly Populated Biological Pathways

Finally, we integrated the metabolomics and proteomics results to reveal pathways abundantly represented in the data using the Joint Pathway Analysis module in MetaboAnalyst [34]. Here, metabolites and proteins were converted to KEGG identifiers and pathways. Out of 310 identified pathways, 25 were considered statistically enriched by hypergeometric test (FDR-corrected $p \leq 0.05$), with many of them corresponding to metabolic processes within the KEGG global metabolic network, including fatty acid metabolism, pentose phosphate pathway, glycolysis and TCA cycle, purine metabolism, and amino acid metabolism (**Figure 2I**). Metabolite-protein constituents of each pathway were identified using MetaboAnalyst and can be mapped for further

14

analysis. To look closer at the identified pathway results, we used the Joint Pathway Analysis module to visualize 55 proteins and 3 general metabolite classes ("branched fatty acids") represented in the fatty acid biosynthesis and degradation pathways (**Figure 2J**). Other metabolic pathways abundantly represented in the dataset includedglycerophospholipid metabolism, oxidative phosphorylation, and cell junction, (i.e. focal adhesion, tight junctions). Pathways involved in protein synthesis such as RNA transport and degradation, and the spliceosome were also abundantly represented (**Figure S12; Table S6**). Together, these results offer holistic insights into which cellular pathways are most active in d42 hPSC-CMs.

Conclusions

Our novel multi-omics strategy for the analysis of metabolites and proteins from the same hPSC-CM monolayer culture enables an integrated assessment of the hPSC-CM proteome and metabolome comprehensively and reproducibly. Benefiting from the rapid metabolite extraction from hPSC-CM cell culture and the facile sample processing for MS analysis, a large number of samples can be extracted and analyzed. We achieved broad coverage of metabolite classes from a rapid methanol extraction of hPSC-CM in culture, including carbohydrates and amino acids to a variety of phospholipids. Strong technical and biological reproducibility was shown by highly similar mass spectra and metabolite annotations. Additionally, we achieved high proteome coverage of the residual hPSC-CM cell pellet, identifying nearly 4,000 proteins per hPSC-CM pellet. Here, we showed consistent recovery of protein from each hPSC-CM monolayer. Using 200 ng per sample, we measured strong correlation of protein intensities from sequentially-extracted cultures. Finally, we mapped identified metabolites and proteins to networks and identified highly-abundant pathways in the dataset. We envision this multi-omics strategy will

provide a technical foundation for future studies on the quantitative evaluation of various hPSC-CM conditions and identification of integrated proteomic and metabolomic markers to advance our understanding of hPSC-CM biology.

Acknowledgements

Author Contributions

E.F.B., A.D.S, D.S.R., Y.Z., and T.J.A. performed the research; E.F.B., A.D.S., D.S.R., Y.Z., T.J.A., B.W., S.P.P. and Y.G. wrote the manuscript.
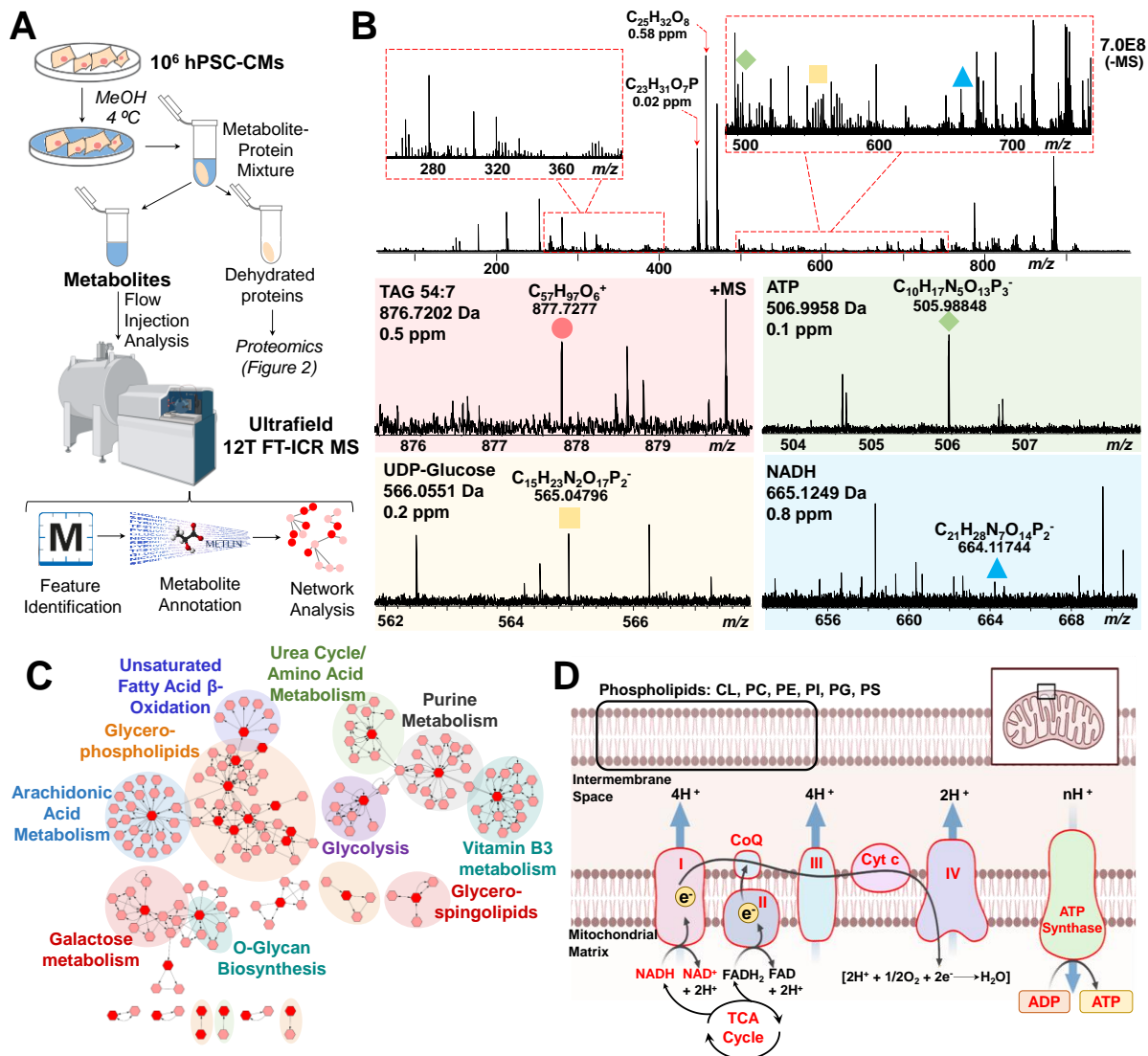
Figure 1. Ultrahigh-resolution mass spectrometry (MS)-based metabolomics of hPSC-CMs.
A) Schematic of the extraction and MS analysis of metabolites from hPSC-CM monolayer culture.
B) Identification of metabolites from complex broadband spectra enabled by FIE-FTICR MS.
Important metabolites are identified with sub-ppm mass accuracy, including stearic acid (upper left), NADH (upper right), UDP-glucose (lower left), and cardiolipin (lower right). **C)** Network analysis of identified metabolites show arachidonic acid metabolism, glycolysis, and glycerophospholipid metabolism pathways represented in the dataset. **D)** Oxidative phosphorylation was well-represented, with a total of 84 protein and metabolite hits within the dataset, highlighted in red. Additionally, many phospholipid species that comprise the mitochondrial membrane were detected, including cardiolipins (CL), phosphocholines (PC), phosphoethanolamines (PE), phosphoinostitols (PI), phosphoglycerols (PG), and phosphatidylserines (PS).
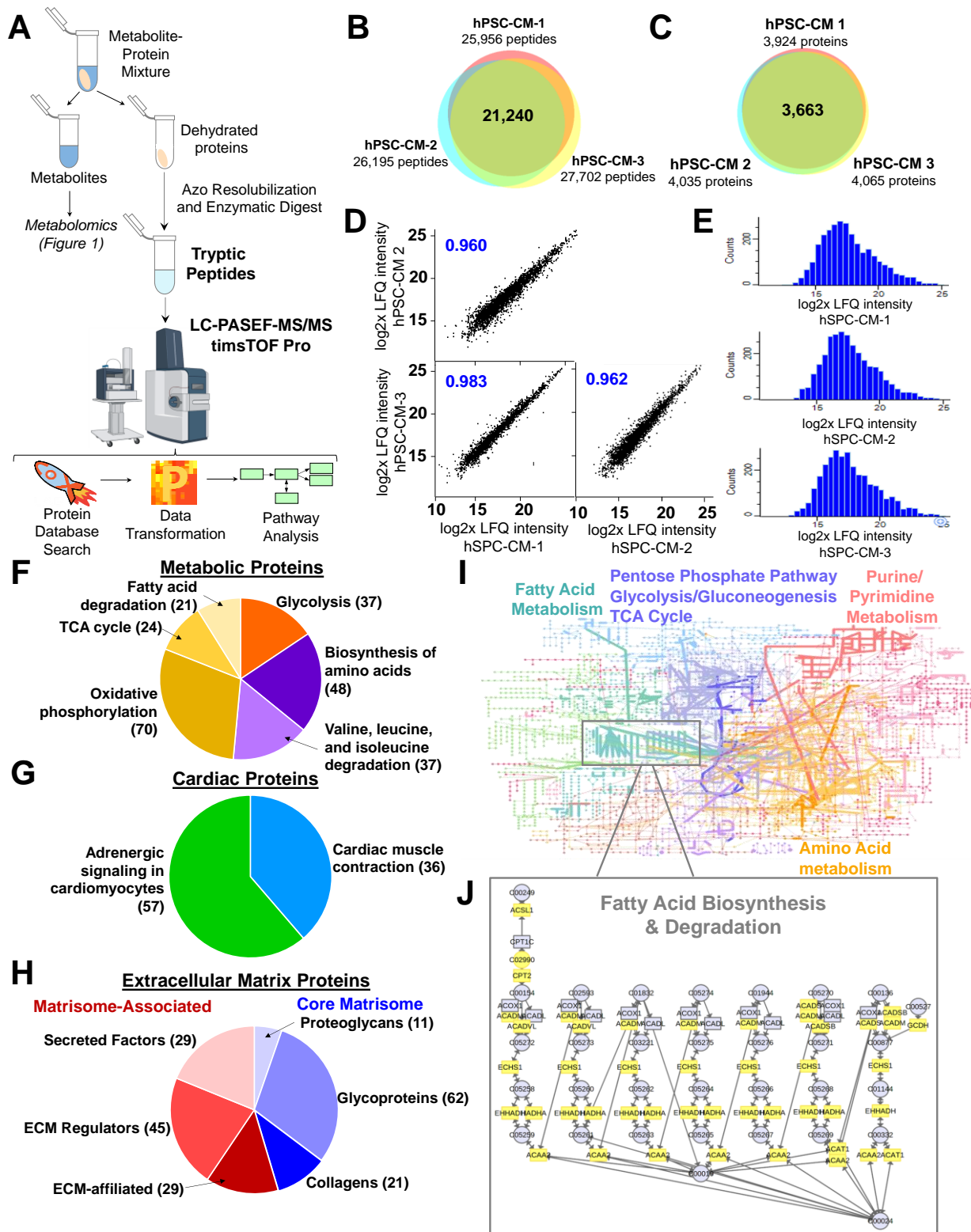
Figure 2. Global proteomics of hPSC-CM cell pellet after metabolomics and pathways revealed by integrated multi-omics analysis. **A)** hPSC-CM proteomics sample preparation workflow starting from the combined metabolite-protein sample. Residual dehydrated cell pellet

is resolubilized in a buffer containing 0.25% Azo, a novel photo-cleavable surfactant proven to access critical membrane proteins. Proteins are enzymatically digested using trypsin before separation by RPLC and analysis by PASEF-enabled timsTOF Pro. Database searching and normalization were performed using MaxQuant, further annotated and visualized using Perseus. Pathway and functional enrichment analysis was performed by DAVID. **B)** Overlap in peptides identified for each sequentially-extracted hPSC-CM biological replicate (n=3). We detected 21,240 shared peptides between three hPSC-CM cultures. **C)** Reproducibility in hPSC-CM biological replicates (n=3). Protein groups identified show 85% overlap between three hPSC-CM monolayer cultures, corresponding to 3,663 protein groups in common. **D)** Log2x-transformed LFQ intensities of shared proteins in each biological replicate show strong correlation between samples, with Pearson correlation coefficients ranging from 0.960-0.983. **E)** Histogram showing normal distribution of log2x-transformed LFQ intensities from sequentially-extracted hPSC-CM biological replicates. **F)** Representative KEGG pathways considered statistically-overrepresented (FDR-corrected $p \leq 0.05$) for Metabolic Proteins **(F)** and Cardiac-specific proteins (**G**). Metabolic proteins included those involved in glycolysis (hsa00010, orange), amino acid metabolism (biosynthesis of amino acids, hsa01230, and valine, leucine, and isoleucine degradation, hsa00280, both purple), and oxidative respiration (oxidative phosphorylation, hsa00190, TCA cycle, hsa00020, and fatty acid degradation, hsa00071, all yellow). Proteins involved in cardiac-specific pathways such as adrenergic signaling of cardiomyocytes (hsa04261, green) and cardiac muscle contraction (hsa04260, blue) were identified. The number of proteins in each pathway is indicated in parentheses. **H)** Extracellular matrix (ECM) proteins were categorized into Core Matrisome (red) and Matrisome-associated proteins (blue). The number of proteins in each category is indicated in parentheses. Core matrisome proteins include proteoglycans, glycoproteins, and collagen species, while matrisome-associated proteins include secreted factors, ECM regulators, and ECM-affiliated proteins. **I)** Visualization of multi-omics metabolism pathways by MetaboAnalyst. Proteomics and metabolomics data were uploaded to MetaboAnalyst for pathway analysis. The Network Analysis module showed significantly-enriched pathways within the KEGG metabolic network for proteins and metabolites, including fatty acid metabolism, amino acid metabolism, purine/pyrimidine metabolism, and glycolysis, pentose phosphate pathway, and TCA cycle. **J)** Zoom panel shows detailed pathways showing detected entities for fatty acid degradation. In total, 58 members of fatty acid degradation pathway were detected, indicated in yellow. KEGG nomenclature is used to describe proteins and metabolites.

References

[1] J. Zhang, F. Wilson Gisela, G. Soerens Andrew, H. Koonce Chad, J. Yu, P. Palecek Sean, A. Thomson James, J. Kamp Timothy, Functional Cardiomyocytes Derived From Human Induced Pluripotent Stem Cells, Circulation Research 104(4) (2009) e30-e41.

[2] P.W. Burridge, Y.F. Li, E. Matsa, H. Wu, S.-G. Ong, A. Sharma, A. Holmström, A.C. Chang, M.J. Coronado, A.D. Ebert, J.W. Knowles, M.L. Telli, R.M. Witteles, H.M. Blau, D. Bernstein, R.B. Altman, J.C. Wu, Human induced pluripotent stem cell–derived cardiomyocytes recapitulate the predilection of breast cancer patients to doxorubicin-induced cardiotoxicity, Nature Medicine 22(5) (2016) 547-556.

[3] L. Ye, Y.-H. Chang, Q. Xiong, P. Zhang, L. Zhang, P. Somasundaram, M. Lepley, C. Swingen, L. Su, Jacqueline S. Wendel, J. Guo, A. Jang, D. Rosenbush, L. Greder, James R. Dutton, J. Zhang, Timothy J. Kamp, Dan S. Kaufman, Y. Ge, J. Zhang, Cardiac Repair in a Porcine Model of Acute Myocardial Infarction with Human Induced Pluripotent Stem Cell-Derived Cardiovascular Cells, Cell Stem Cell 15(6) (2014) 750-761.

[4] E. Matsa, P.W. Burridge, J.C. Wu, Human stem cells for modeling heart disease and for drug discovery, Science translational medicine 6(239) (2014) 239ps6-239ps6.

[5] B.J. van Meer, L.G.J. Tertoolen, C.L. Mummery, Concise Review: Measuring Physiological Responses of Human Pluripotent Stem Cell Derived Cardiomyocytes to Drugs and Disease, Stem cells (Dayton, Ohio) 34(8) (2016) 2008-2015.

[6] X. Lian, C. Hsiao, G. Wilson, K. Zhu, L.B. Hazeltine, S.M. Azarin, K.K. Raval, J. Zhang, T.J. Kamp, S.P. Palecek, Robust cardiomyocyte differentiation from human pluripotent stem cells via temporal modulation of canonical Wnt signaling, Proceedings of the National Academy of Sciences 109(27) (2012) E1848.

[7] P.W. Burridge, E. Matsa, P. Shukla, Z.C. Lin, J.M. Churko, A.D. Ebert, F. Lan, S. Diecke, B. Huber, N.M. Mordwinkin, J.R. Plews, O.J. Abilez, B. Cui, J.D. Gold, J.C. Wu, Chemically defined generation of human cardiomyocytes, Nature Methods 11(8) (2014) 855-860.

[8] M. Waas, R. Weerasekera, E.M. Kropp, M. Romero-Tejeda, E.N. Poon, K.R. Boheler, P.W. Burridge, R.L. Gundry, Are These Cardiomyocytes? Protocol Development Reveals Impact of Sample Preparation on the Accuracy of Identifying Cardiomyocytes by Flow Cytometry, Stem Cell Reports 12(2) (2019) 395-410.

[9] E. Karbassi, A. Fenix, S. Marchiano, N. Muraoka, K. Nakamura, X. Yang, C.E. Murry, Cardiomyocyte maturation: advances in knowledge and implications for regenerative medicine, Nature Reviews Cardiology 17(6) (2020) 341-359.

[10] N.T. Feric, M. Radisic, Maturing human pluripotent stem cell-derived cardiomyocytes in human engineered cardiac tissues, Advanced Drug Delivery Reviews 96 (2016) 110-134.

[11] K. Ronaldson-Bouchard, S.P. Ma, K. Yeager, T. Chen, L. Song, D. Sirabella, K. Morikawa, D. Teles, M. Yazawa, G. Vunjak-Novakovic, Advanced maturation of human cardiac tissue grown from pluripotent stem cells, Nature 556(7700) (2018) 239-243.

[12] W. Cai, J. Zhang, W.J. de Lange, Z.R. Gregorich, H. Karp, E.T. Farrell, S.D. Mitchell, T. Tucholski, Z. Lin, M. Biermann, S.J. McIlwain, J.C. Ralphe, T.J. Kamp, Y. Ge, An Unbiased Proteomics Method to Assess the Maturation of Human Pluripotent Stem Cell–Derived Cardiomyocytes, Circulation Research 125 (2019) 936-953.

[13] J.A. Melby, W.J. de Lange, J. Zhang, D.S. Roberts, S.D. Mitchell, T. Tucholski, G. Kim, A. Kyrvasilis, S.J. McIlwain, T.J. Kamp, J.C. Ralphe, Y. Ge, Functionally Integrated Top-Down Proteomics for Standardized Assessment of Human Induced Pluripotent Stem Cell-Derived Engineered Cardiac Tissues, Journal of Proteome Research 20(2) (2021) 1424-1433.

[14] E.S. Nakayasu, C.D. Nicora, A.C. Sims, K.E. Burnum-Johnson, Y.-M. Kim, J.E. Kyle, M.M. Matzke, A.K. Shukla, R.K. Chu, A.A. Schepmoes, J.M. Jacobs, R.S. Baric, B.-J. Webb-Robertson, R.D. Smith, T.O. Metz, MPLEx: a Robust and Universal Protocol for Single-Sample Integrative Proteomic, Metabolomic, and Lipidomic Analyses, mSystems 1(3) (2016) e00043-16.

[15] C. Coman, F.A. Solari, A. Hentschel, A. Sickmann, R.P. Zahedi, R. Ahrends, Simultaneous Metabolite, Protein, Lipid Extraction (SIMPLEX): A Combinatorial Multimolecular Omics Approach for Systems Biology, Molecular & cellular proteomics : MCP 15(4) (2016) 1453-1466.

[16] K.J. Karczewski, M.P. Snyder, Integrative omics for health and disease, Nature Reviews Genetics 19(5) (2018) 299-310.

[17] A. Joshi, M. Rienks, K. Theofilatos, M. Mayr, Systems biology in cardiovascular disease: a multiomics approach, Nature Reviews Cardiology (2020).

[18] M. Mayr, B. Madhu, Q. Xu, Proteomics and Metabolomics Combined in Cardiovascular Research, Trends in Cardiovascular Medicine 17(2) (2007) 43-48.

[19] W. McGarrah Robert, B. Crown Scott, G.-F. Zhang, H. Shah Svati, B. Newgard Christopher, Cardiovascular Metabolomics, Circulation Research 122(9) (2018) 1238-1258.

[20] F.R. Pinu, D.J. Beale, A.M. Paten, K. Kouremenos, S. Swarup, H.J. Schirra, D. Wishart, Systems Biology and Multi-Omics Integration: Viewpoints from the Metabolomics Research Community, Metabolites 9(4) (2019).

[21] X. Lian, J. Zhang, S.M. Azarin, K. Zhu, L.B. Hazeltine, X. Bao, C. Hsiao, T.J. Kamp, S.P. Palecek, Directed cardiomyocyte differentiation from human pluripotent stem cells by modulating Wnt/β-catenin signaling under fully defined conditions, Nature Protocols 8(1) (2013) 162-175.

[22] Q. Teng, W. Huang, T.W. Collette, D.R. Ekman, C. Tan, A direct cell quenching method for cell-culture based metabolomics, Metabolomics 5(2) (2008) 199.

[23] K.A. Brown, T. Tucholski, C. Eken, S. Knott, Y. Zhu, S. Jin, Y. Ge, High-Throughput Proteomics Enabled by a Photocleavable Surfactant, Angewandte Chemie International Edition 59(22) (2020) 8406-8410.

[24] Y. Zhu, B. Wancewicz, M. Schaid, T.N. Tiambeng, K. Wenger, Y. Jin, H. Heyman, C.J. Thompson, A. Barsch, E.D. Cox, D.B. Davis, A.R. Brasier, M.E. Kimple, Y. Ge, Ultrahigh-Resolution Mass Spectrometry-Based Platform for Plasma Metabolomics Applied to Type 2 Diabetes Research, Journal of Proteome Research 20(1) (2021) 463-473.

[25] D.S. Wishart, Y.D. Feunang, A. Marcu, A.C. Guo, K. Liang, R. Vázquez-Fresno, T. Sajed, D. Johnson, C. Li, N. Karu, Z. Sayeeda, E. Lo, N. Assempour, M. Berjanskii, S. Singhal, D. Arndt, Y. Liang, H. Badran, J. Grant, A. Serra-Cayuela, Y. Liu, R. Mandal, V. Neveu, A. Pon, C. Knox, M. Wilson, C. Manach, A. Scalbert, HMDB 4.0: the human metabolome database for 2018, Nucleic Acids Research 46(D1) (2018) D608-D617.

[26] T. Kind, K.-H. Liu, D.Y. Lee, B. DeFelice, J.K. Meissen, O. Fiehn, LipidBlast in silico tandem mass spectrometry database for lipid identification, Nature Methods 10(8) (2013) 755-758.

[27] C. Guijas, J.R. Montenegro-Burke, X. Domingo-Almenara, A. Palermo, B. Warth, G. Hermann, G. Koellensperger, T. Huan, W. Uritboonthai, A.E. Aisporna, D.W. Wolan, M.E. Spilker, H.P. Benton, G. Siuzdak, METLIN: A Technology Platform for Identifying Knowns and Unknowns, Analytical Chemistry 90(5) (2018) 3156-3164.

[28] T. Hulsen, J. de Vlieg, W. Alkema, BioVenn – a web application for the comparison and visualization of biological lists using area-proportional Venn diagrams, BMC Genomics 9(1) (2008) 488.

[29] J. Gao, V.G. Tarcea, A. Karnovsky, B.R. Mirel, T.E. Weymouth, C.W. Beecher, J.D. Cavalcoli, B.D. Athey, G.S. Omenn, C.F. Burant, H.V. Jagadish, Metscape: a Cytoscape plug-in for visualizing and interpreting metabolomic data in the context of human metabolic networks, Bioinformatics 26(7) (2010) 971-973.

[30] F. Meier, A.-D. Brunner, S. Koch, H. Koch, M. Lubeck, M. Krause, N. Goedecke, J. Decker, T. Kosinski, M.A. Park, N. Bache, O. Hoerning, J. Cox, O. Räther, M. Mann, Online Parallel Accumulation–Serial Fragmentation (PASEF) with a Novel Trapped Ion Mobility Mass Spectrometer, Molecular & Cellular Proteomics 17(12) (2018) 2534-2545.

[31] N. Prianichnikov, H. Koch, S. Koch, M. Lubeck, R. Heilig, S. Brehmer, R. Fischer, J. Cox, MaxQuant Software for Ion Mobility Enhanced Shotgun Proteomics*, Molecular & Cellular Proteomics 19(6) (2020) 1058-1069.

21

[32] S. Tyanova, J. Cox, Perseus: A Bioinformatics Platform for Integrative Analysis of Proteomics Data in Cancer Research, in: L. von Stechow (Ed.), Cancer Systems Biology: Methods and Protocols, Springer New York, New York, NY, 2018, pp. 133-148.

[33] B. Jassal, L. Matthews, G. Viteri, C. Gong, P. Lorente, A. Fabregat, K. Sidiropoulos, J. Cook, M. Gillespie, R. Haw, F. Loney, B. May, M. Milacic, K. Rothfels, C. Sevilla, V. Shamovsky, S. Shorser, T. Varusai, J. Weiser, G. Wu, L. Stein, H. Hermjakob, P. D'Eustachio, The reactome pathway knowledgebase, Nucleic Acids Research 48(D1) (2020) D498-D503.

[34] J. Chong, O. Soufan, C. Li, I. Caraus, S. Li, G. Bourque, D.S. Wishart, J. Xia, MetaboAnalyst 4.0: towards more transparent and integrative metabolomics analysis, Nucleic Acids Research 46(W1) (2018) W486-W494.

[35] K. Dettmer, N. Nürnberger, H. Kaspar, M.A. Gruber, M.F. Almstetter, P.J. Oefner, Metabolite extraction from adherently growing mammalian cells for metabolomics studies: optimization of harvesting and extraction protocols, Analytical and Bioanalytical Chemistry 399(3) (2011) 1127-1139.

[36] K.A. Brown, B. Chen, T.M. Guardado-Alvarez, Z. Lin, L. Hwang, S. Ayaz-Guner, S. Jin, Y. Ge, A photocleavable surfactant for top-down proteomics, Nature Methods 16(5) (2019) 417-420.

[37] T.J. Aballo, D.S. Roberts, J.A. Melby, K.M. Buck, K.A. Brown, Y. Ge, Ultrafast and Reproducible Proteomics from Small Amounts of Heart Tissue Enabled by Azo and timsTOF Pro, bioRxiv (2021) 2021.05.24.445470.

[38] F. Meier, S. Beck, N. Grassl, M. Lubeck, M.A. Park, O. Raether, M. Mann, Parallel Accumulation–Serial Fragmentation (PASEF): Multiplying Sequencing Speed and Sensitivity by Synchronized Scans in a Trapped Ion Mobility Device, Journal of Proteome Research 14(12) (2015) 5378-5387.

[39] F. Meier, A.-D. Brunner, S. Koch, H. Koch, M. Lubeck, M. Krause, N. Goedecke, J. Decker, T. Kosinski, M.A. Park, N. Bache, O. Hoerning, J. Cox, O. Räther, M. Mann, Online Parallel Accumulation–Serial Fragmentation (PASEF) with a Novel Trapped Ion Mobility Mass Spectrometer *^{		}, Molecular & Cellular Proteomics 17(12) (2018) 2534-2545.

[40] G.D. Lopaschuk, J.S. Jaswal, Energy Metabolic Phenotype of the Cardiomyocyte During Development, Differentiation, and Postnatal Maturation, Journal of Cardiovascular Pharmacology 56(2) (2010).

[41] C. Kolwicz Stephen, S. Purohit, R. Tian, Cardiac Metabolism and its Interactions With Contraction, Growth, and Survival of Cardiomyocytes, Circulation Research 113(5) (2013) 603-616.

[42] D.K. Reibel, B. O'Rourke, K.A. Foster, H. Hutchinson, C.E. Uboh, R.L. Kent, Altered phospholipid metabolism in pressure-overload hypertrophied hearts, American Journal of Physiology-Heart and Circulatory Physiology 250(1) (1986) H1-H6.

[43] D.W. Huang, B.T. Sherman, R.A. Lempicki, Systematic and integrative analysis of large gene lists using DAVID bioinformatics resources, Nature Protocols 4(1) (2009) 44-57.

[44] R. Forough, C. Scarcello, M. Perkins, Cardiac biomarkers: a focus on cardiac regeneration, The journal of Tehran Heart Center 6(4) (2011) 179-186.

[45] G.J. Scuderi, J. Butcher, Naturally Engineered Maturation of Cardiomyocytes, Frontiers in Cell and Developmental Biology 5 (2017) 50.

[46] A. Naba, K.R. Clauser, H. Ding, C.A. Whittaker, S.A. Carr, R.O. Hynes, The extracellular matrix: Tools and insights for the "omics" era, Matrix Biology 49 (2016) 10-24.

[47] C.W. Chang, A.J. Dalgliesh, J.E. López, L.G. Griffiths, Cardiac extracellular matrix proteomics: Challenges, techniques, and clinical implications, PROTEOMICS – Clinical Applications 10(1) (2016) 39-50.

[48] S.J. Knott, K.A. Brown, H. Josyer, A. Carr, D. Inman, S. Jin, A. Friedl, S.M. Ponik, Y. Ge, Photocleavable Surfactant-Enabled Extracellular Matrix Proteomics, Analytical Chemistry 92(24) (2020) 15693-15698.